Polynomial-Method-Based Design of Low-Order Controllers for Two-Mass Systems

Chengbin Ma, *Member, IEEE*, Junyi Cao, and Yue Qiao

***Abstract*—In this paper, low-order integral–proportional (IP), modified IP (m-IP), and modified integral–proportional–derivative (m-IPD) controllers are designed for the speed control of a two-mass system based on a normalized model and polynomial method. In order to have sufficient damping, the parameters of the controllers are determined through characteristic-ratio assignment under the principle that all the characteristic ratios should be larger than two. It is found that for an inertia ratio smaller than one-third, an IP controller can effectively suppress the vibrations with proper damping, while for a relatively larger inertia ratio, an m-IP controller (i.e., IP controller with an additional low-pass filter) is effective. m-IPD control is theoretically effective for a large inertia ratio. However, the necessity of a negative derivative gain leads to a very poor robustness. Both simulation and experimental results verified the effectiveness of the designed IP and m-IP controllers when the inertia ratio is relatively small. For the m-IPD controller, its poor robustness is demonstrated by introducing a large gear backlash in experiments, while the IP and m-IP controllers show promising results of a much better robustness against the gear backlash nonlinearity.**

***Index Terms*—Low-order controller, polynomial method, speed control, two-mass system.**

I. Introduction

ELECTRIC motors are one of the most widely used actuators in industry today, which can be found nearly in all the electromechanical systems, such as robots, machine tools, hard disks, etc. The proliferation of electric motors is still continuing, particularly in the area of alternative energy systems such as electric vehicles and wind turbine generators. The capability of the high-bandwidth speed control of electric motors greatly improves the responses of the drive systems. However, it may also easily excite mechanical vibrations, which are the major obstacles for achieving the high-performance control of the systems. These mechanical vibrations are caused by several mechanical elements such as elastic shaft, gear backlash, and coupling. The mechanical vibrations can be observed in the speed control of many electric drive systems from the traditional applications such as in steel rolling mills and elevators to the latest ones in electric vehicles and wind turbines, etc. [1].

The aforementioned systems are usually being modeled as multimass systems. However, the analysis of a typical benchmark, a two-mass system, also gives a good starting point and fruitful results for dealing with more complex systems. In the typical benchmark two-mass control problem, it is usually assumed that only the velocity of the drive side is measurable, whereas the driving torque, load torque, and the velocity of the load side are not measurable. The designed controller needs to control the velocity of the load side within well-suppressed vibrations using only the velocity feedback of the drive side. The vibration suppression for the two-mass system has attracted the attention of many researchers during the past decade. A two-degree-of-freedom control structure using an observer-based state feedback compensator was proposed to suppress the mechanical vibrations in rolling mill drives [2]. A vibration suppression control method was reported, which is based on the feedback of the imperfect derivative of the torsional torque estimated by a disturbance observer [3]. A μ-synthesis with a descriptor form representation was proposed for an active vibration control of the two-mass system, which can achieve both the robust stability and robust disturbance suppression [4]. A series antiresonance finite-impulse response compensator was applied to filter torque command signal for a passive vibration control in a high-performance speed servo drive [5]. The controller structures and their parameters were discussed based on the ratio between load and drive inertias and delay in speed control loop for an active damping of torsional vibrations [6].

In recent years, intelligent control has begun to be applied in the vibration control of the two-mass system. A dynamically generated fuzzy neural network was applied to control the torsional vibrations of tandem cold-rolling mill spindles, which can be modeled as a two-mass system [7]. A universal approximator based on a radial basis function network was introduced to the speed control of the two-mass system, which has a self-learning capability compared with the inverse model-based disturbance observer [8]. It was reported that an adaptive neuro-fuzzy controller can also be applied to suppress the torsional vibrations of the two-mass system [9], while neural networks were introduced to estimate the torsional torque and the load-side speed for the damping of the torsional vibrations of the two-mass system [10]. A sliding-mode neuro-fuzzy controller was used as an adaptive speed controller to damp the torsional vibrations in the two-mass system [11].

As explained earlier, generally, the controller design of the two-mass system falls into control problems treated by modern

Manuscript received July 3, 2010; revised December 3, 2010, March 28, 2011, July 3, 2011, and September 28, 2011; accepted February 8, 2012. Date of publication February 24, 2012; date of current version October 16, 2012. This work was supported by the National Science Foundation of China [Grants 50905113 (2010–2012) and 50805113 (2009–2011)].

C. Ma and Y. Qiao are with the University of Michigan–Shanghai Jiao Tong University Joint Institute, Shanghai Jiao Tong University, Shanghai 200240, China (e-mail: chbma@sjtu.edu.cn; qiaoyue@sjtu.edu.cn).

J. Cao is with the School of Mechanical Engineering, Xi'an Jiaotong University, Xi'an 710049, China (e-mail: caojy@mail.xjtu.edu.cn).

Digital Object Identifier 10.1109/TIE.2012.2188869

control theory, which usually leads to complicated high-order controllers with difficulties in weighting function selection, parameter tuning, etc. [2]–[5]. However, the dominant control structures working in the electric drive industry are based on the low-order PID controllers and their modifications. It is both theoretically and practically important to further improve the PID design for the vibration suppression control of the two-mass system, which would significantly contribute to the real industrial applications.

In addition to the well-known classical control and modern control for the controller design, there is actually a third approach called algebraic design approach that uses polynomial expressions (i.e., polynomial method). In this approach, the type and order of the controller and its corresponding characteristic polynomial of the closed-loop control system are defined at the beginning. Then, the coefficients of the polynomial can be determined considering certain design specifications. Therefore, in this paper, the polynomial method is introduced to design the low-order PID controllers via the so-called characteristic-ratio assignment [12], [13]. It was observed that the set of characteristic ratios has a strong relationship with the damping of a system. Furthermore, the transient response can also be directly addressed based on the relationships between the characteristic ratios and time-domain responses. Naslin empirically observed these relationships in the 1960s [14]. An important contribution is attributed to Manabe, who proposed the coefficient diagram method (CDM) based on Naslin's findings and the Lipatov–Sokolov stability criterion [15]. Using the CDM method, he designed controllers for many successful industrial applications.

The purpose of this paper is to explore the possibility of using the polynomial method to improve the low-order PID controller design for the vibration suppression control of the two-mass system. The controller design with various PID structures, integral–proportional (IP), modified IP (m-IP), and modified integral–proportional–derivative (m-IPD), is discussed by specifying a certain set of characteristic ratios, when the inertia ratio (i.e., the ratio of drive inertia to the total inertia) varies. From a theoretical viewpoint, the research on the polynomial-method-based controller design is still in its beginning stage. This paper represents one of the initial efforts to systematically apply the polynomial method in a challenging benchmark problem, the vibration suppression of the two-mass system. Theoretical analysis and simulation results in this paper were confirmed by experimental tests using a laboratory torsion test bench.

II. Normalization and Stability Analysis

The two-mass system can be modeled as two masses being connected by a nonstiff coupling shaft as shown in Fig. 1, where K_s is the spring coefficient and J_m and J_l are the inertias of the drive (including the drive motor) and load sides, respectively. From its block diagram, the transfer function between the driving torque T_m and the angular velocity of the drive side ω_m can be derived as

$$P(s) = \frac{s^2 + \omega_a^2}{J_m s\left(s^2 + \omega_r^2\right)} \tag{1}$$

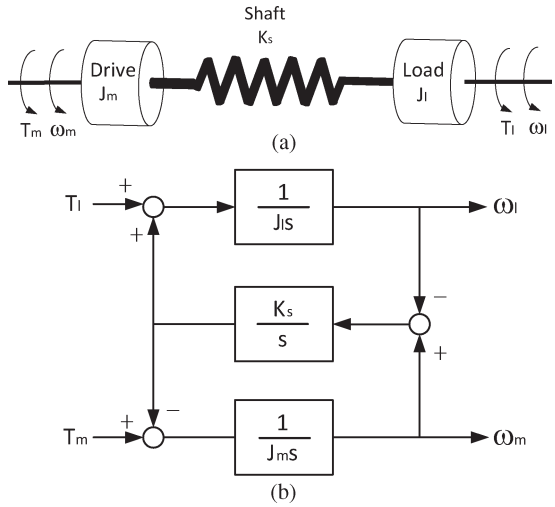

Fig. 1. Modeling of the two-mass system. (a) Model. (b) Block diagram.

where ω_r and ω_a are the resonance frequency and antiresonance frequency, respectively,

$$\omega_r = \sqrt{K_s\left(\frac{1}{J_m} + \frac{1}{J_l}\right)} \tag{2}$$

$$\omega_a = \sqrt{\frac{K_s}{J_l}}. \tag{3}$$

In order to have a generalized discussion, the transfer function $P(s)$ can be normalized by substituting the original Laplace operator s with s^*, which is equal with s/ω_a. The transfer function after normalization is

$$\frac{q}{J_m}\frac{1}{\omega_a}\frac{s^{*2}+1}{qs^{*3}+s^*} \tag{4}$$

where q is the inertia ratio which is defined as the ratio of drive inertia to the total inertia

$$q = \frac{J_m}{J_m + J_l}. \tag{5}$$

As shown in Fig. 2, the three types of PID controllers, IP controller, m-IP controller, and m-IPD controller, are discussed for the speed control of the two-mass system. Unlike the classical PID controllers, an alternative configuration called setpoint-on-I-only configuration is adopted to smooth the discontinuity of the reference command ω_r by the integral (i.e., the I controller). In order to distinguish these special PID controllers from the classical PID controllers, they are usually named as IP or IPD controllers. And the prefix "m" (i.e., modified) refers to the introduction of the first-order low-pass filter $1/(T_d s + 1)$ in the controllers, as shown in Fig. 2(b) and (c). For the sake of simplicity, the normalized model for the two-mass system is taken as

$$P_n(s^*) = \frac{s^{*2}+1}{qs^{*3}+s^*}. \tag{6}$$

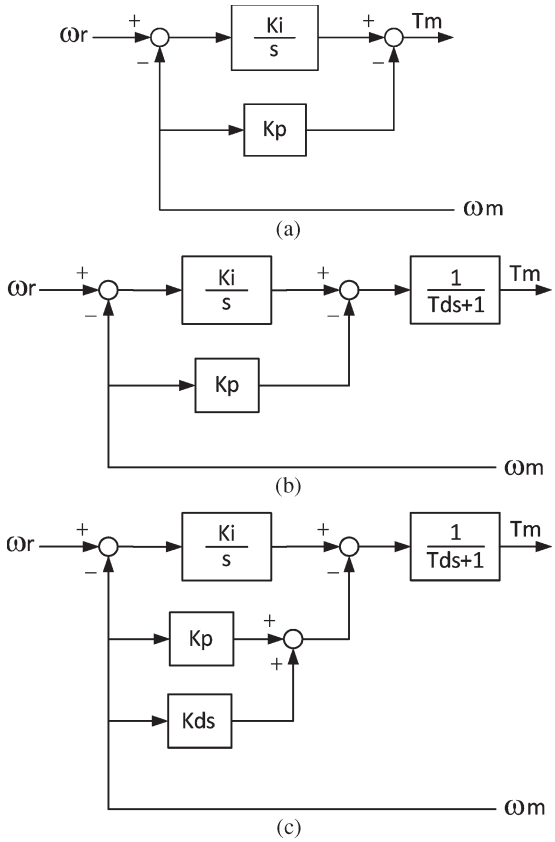

Fig. 2. PID controllers for the speed control of the two-mass system. (a) IP controller. (b) m-IP controller. (c) m-IPD controller.

By comparing (6) with (4), the controller parameters K_p, K_i, K_d, and T_d can be calculated as

$$K_p = K_p^* \frac{J_m \omega_a}{q} \tag{7}$$

$$K_i = K_i^* \frac{J_m \omega_a^2}{q} \tag{8}$$

$$K_d = K_d^* \frac{J_m}{q} \tag{9}$$

$$T_d = \frac{T_d^*}{\omega_a} \tag{10}$$

where K_p^*, K_i^*, K_d^*, and T_d^* are the controller parameters designed using the simplified normalized model (6). Compared with the time response of the normalized system, the real response is sped up by a factor of ω_a, which is straightforward from the Laplace transform of time-scaled functions.

TABLE I
ROUTH'S TABULATION

s^{*4}	q	$(1+K_i^*)$	K_i^*
s^{*3}	K_p^*	K_p^*	0
s^{*2}	$(1+K_i^*)-q$	K_i^*	0
s^{*1}	$\frac{K_p^*(1-q)}{(1+K_i^*)-q}$	0	0
s^{*0}	K_i^*	0	0

The closed-loop transfer function for the IP feedback control loop is

$$G_n(s^*) = \frac{K_i^*(s^{*2}+1)}{q s^{*4} + K_p^* s^{*3} + (1+K_i^*)\, s^{*2} + K_p^* s^* + K_i^*}. \tag{11}$$

From the Routh's tabulation for the characteristic equation, as shown in Table I, it is interesting to notice that the stability condition is

$$0 < q < 1 \tag{12}$$

with positive K_i^* and K_p^*. Obviously, for the two-mass system, the inertia ratio q is always a positive number smaller than one. However, $1-q$ can be considered as a stability margin. It is clear to see that a large inertia ratio q will lead to a deteriorated stability.

For the m-IP control loop, its closed-loop transfer function is (13), shown at the bottom of the page. Again, from Routh–Hurwitz criterion, the closed control loop is stable if and only if $K_p^* - T_d^* K_i^* > 0$ and $1-q>0$ with positive K_p^*, K_i^*, and T_d^*.

Similarly, the closed-loop transfer function of the m-IPD control loop is (14), shown at the bottom of the page. Unlike the IP and m-IP control loops, its stability condition is very complicated. As in the following sections, the m-IPD controller is only needed when q is larger than 0.6. However, the positive feedback of the D control signal (i.e., a negative K_d^*) becomes necessary, which makes the m-IPD controller impractical for real applications due to its very poor robustness.

III. Design Via Characteristic-Ratio Assignment

For a Hurwitz polynomial with real positive coefficients

$$p(s) = a_n s^n + a_{n-1} s^{n-1} + \cdots + a_1 s + a_0 \tag{15}$$

$$G_n(s^*) = \frac{K_i^*(s^{*2}+1)}{T_d^* q s^{*5} + q s^{*4} + \left(T_d^* + K_p^*\right) s^{*3} + (1+K_i^*)\, s^{*2} + K_p^* s^* + K_i^*} \tag{13}$$

$$G_n(s^*) = \frac{K_i^*(s^{*2}+1)}{q T_d^* s^{*5} + (q+K_d^*)\, s^{*4} + \left(T_d^* + K_p^*\right) s^{*3} + (1+K_i^*+K_d^*)\, s^{*2} + K_p^* s^* + K_i^*} \tag{14}$$

the so-called characteristic ratios are defined as

$$\gamma_1 = \frac{a_1^2}{a_0 a_2}, \quad \gamma_2 = \frac{a_2^2}{a_3 a_1}, \ldots, \gamma_{n-1} = \frac{a_{n-1}^2}{a_{n-2} a_n}. \tag{16}$$

Let $G(s)$ be an all-pole transfer function

$$G(s) = \frac{a_0}{p(s)} = \frac{a_0}{a_n s^n + a_{n-1} s^{n-1} + \ldots + a_1 s + a_0}, \quad a_i > 0 \tag{17}$$

and γ_i be the characteristic ratios of $p(s)$. Then, $G(s)$ has a monotonically decreasing magnitude of frequency response if $\gamma_i > 2$ for all $i = 1, 2, \ldots, n-1$; therefore, the step response overshoot is guaranteed to be small [12]. This result can be utilized to achieve the desired damping by assigning the characteristic ratios γ_i, in which the larger values of γ_i correspond to a greater damping.

For the two-mass system, additional limitations arise from the presence of the two resonance modes (i.e., one pair of $j\omega$-axis zeros and one pair of $j\omega$-axis poles), which makes it difficult to obtain a sufficient damping of the control system. Compared with the all-pole systems, larger characteristic ratios, particularly a larger γ_1, would be required in the controller design for the two-mass system because the characteristic ratios with lower indices i have a dominant influence on time-domain specifications such as the overshoot [13].

A. IP Controller

The design of IP controller, namely, determining K_i^* and K_p^*, can be based on the characteristic-ratio assignment. Due to the existence of the resonance modes, the challenge for the control design of the two-mass system is to maintain a balanced tradeoff between stability and sufficient damping for resonance vibration suppression, particularly when the inertia ratio q is large, while robustness against parameter variations, modeling error, and disturbance is also important.

From the characteristic equation of the IP control loop (11), the characteristic ratios are

$$\gamma_1 = \frac{K_p^{*2}}{K_i^* (1 + K_i^*)} > 2 \tag{18}$$

$$\gamma_2 = \frac{(1 + K_i^*)^2}{K_p^{*2}} > 2 \tag{19}$$

$$\gamma_3 = \frac{K_p^{*2}}{q (1 + K_i^*)} > 2 \tag{20}$$

where the condition of $\gamma_i > 2$ $(i = 1, 2, 3)$ is desired for having a sufficient damping. Through multiplying each side of (19) by the corresponding side of (20), it can be found that

$$q < \frac{1 + K_i^*}{4} \tag{21}$$

while based on (18) and (19), K_i^* should be smaller than one-third. Therefore, in order to let all the characteristic ratios γ_i be larger than two, the inertia ratio q should be restricted as

$$q < \frac{1}{3} \approx 0.333. \tag{22}$$

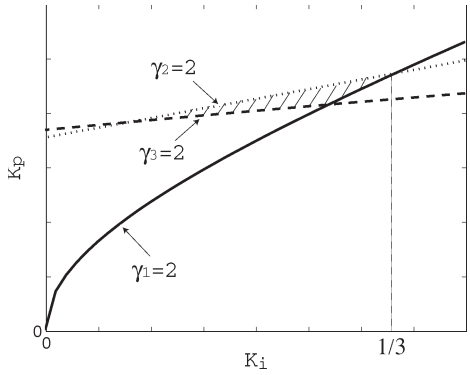

Fig. 3. Overlapped area formed by $\gamma_1 > 2$, $\gamma_2 > 2$, and $\gamma_3 > 2$.

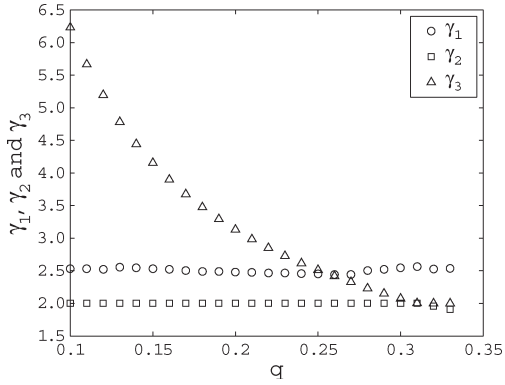

Fig. 4. γ_1, γ_2, and γ_3 with the selected K_i^* and K_p^*.

A graphical method can also be introduced to plot the entire possible combinations of (K_i^*, K_p^*), by which all the characteristic ratios γ_i are larger than two. As shown in Fig. 3, all these combinations are located in the overlapped area formed by the areas of $\gamma_1 > 2$, $\gamma_2 > 2$, and $\gamma_3 > 2$. Among the characteristic ratios, only γ_3 is affected by the inertia ratio q. With an increasing q, the overlapped area will shrink and eventually disappear. The intersection point between the curves of $\gamma_1 = 2$ and $\gamma = 2$ is (1/3, $\sqrt{8/9}$). In addition, if q is larger than one-third, there will be no overlapped area.

In order to guarantee sufficient damping, the combinations of (K_i^*, K_p^*) for having zero-overshoot step time responses are searched by numerical simulation, in which q increases from 0.1 to 0.33. Since a larger K_i^* is desired for a faster time response, K_i^* is decreased from one-third to zero during the searching. Then, with the specific q and K_i^*, the values of K_p^* can be determined by letting $\gamma_1 = 2$, $\gamma_2 = 2$, and $\gamma_3 = 2$. Namely, the desired combinations of K_i^* and K_p^* are selected, by which the time responses have zero overshoot and K_i^* takes on its maximum possible value. As shown in Fig. 4, it is interesting to notice that with the selected K_i^* and K_p^*, γ_1 varies around 2.5 for various q's, and the desired γ_2 is almost two. Only when q is close to one-third, the γ_2 and γ_3 become smaller than two. This observation is actually identical with the standard form of the CDM method, which is based on intensive experimental studies [15].

Therefore, the determination of an initial parameter setting for the IP controller can be simplified as choosing $\gamma_1 = 2.5$ and

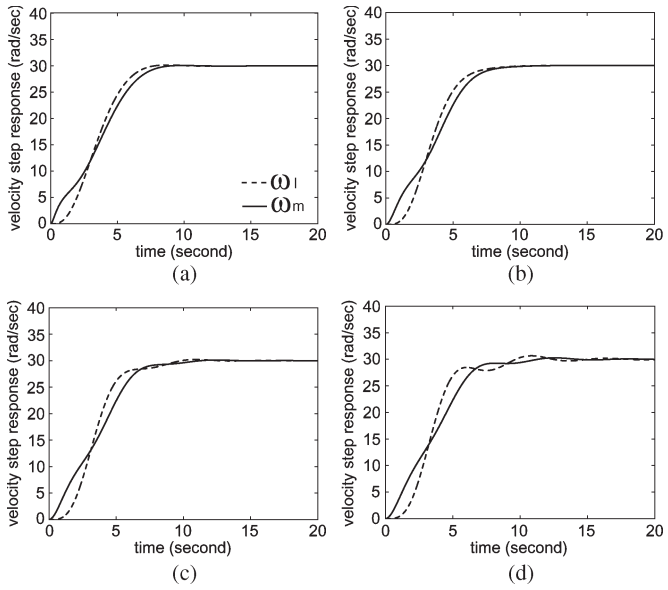

Fig. 5. Velocity step responses with various q's by IP control. (a) $q = 0.1$. (b) $q = 1/3$. (c) $q = 0.5$. (d) $q = 0.6$.

$\gamma_2 = 2$. Namely, based on (18) and (19), K_i^* and K_p^* can be selected as follows when $q < 1/3$:

$$K_i^* = \frac{1}{4}, \quad K_p^* = \frac{5}{4\sqrt{2}}. \tag{23}$$

The step responses of the normalized closed-loop IP control systems are shown in Fig. 5 with the aforementioned initial setting of K_i^* and K_p^*. When q is small, the designed IP controller demonstrates a good performance with zero or nearly zero overshoot and strong robustness against the variation of q. However, with larger q, such as 0.5 and 0.6, it can be seen that the IP controller is not able to provide sufficient damping any more, and the step responses become oscillatory.

B. m-IP Controller

In order to improve the damping when inertia ratio q is larger than one-third, a low-pass filter can be added to the IP controller. Such IP controller with a low-pass filter is called m-IP controller, as shown in Fig. 2(b). Again, from the characteristic equation (13), the characteristic ratios for the m-IP control loop are

$$\gamma_1 = \frac{K_p^{*2}}{K_i^*\left(1 + K_i^*\right)} \tag{24}$$

$$\gamma_2 = \frac{\left(1 + K_i^*\right)^2}{K_p^*\left(K_p^* + T_d^*\right)} \tag{25}$$

$$\gamma_3 = \frac{\left(T_d^* + K_p^*\right)^2}{q\left(1 + K_i^*\right)} \tag{26}$$

$$\gamma_4 = \frac{q}{T_d^*\left(T_d^* + K_p^*\right)}. \tag{27}$$

Let $T_d^* \doteq xK_p^*(x > 0)$ and $\gamma_i > 2$ $(i = 1,\ 2,\ 3,\ 4)$, then

$$\frac{K_p^{*2}}{K_i^*\left(1 + K_i^*\right)} > 2 \tag{28}$$

$$\frac{\left(1 + K_i^*\right)^2}{K_p^{*2}(1 + x)} > 2 \tag{29}$$

$$\frac{K_p^{*2}(1 + x)^2}{q\left(1 + K_i^*\right)} > 2 \tag{30}$$

$$\frac{q}{xK_p^{*2}(1 + x)} > 2. \tag{31}$$

From (28) and (31), the following inequality can be obtained:

$$\frac{q}{K_i^*\left(1 + K_i^*\right)x(1 + x)} > 4. \tag{32}$$

Similarly,

$$\frac{\left(1 + K_i^*\right)(1 + x)}{q} > 4 \tag{33}$$

which is obtained from (29) and (30). Therefore, the relationship between x and K_i^* can be represented as

$$xK_i^* < \frac{1}{16}. \tag{34}$$

In addition, from (30) and (31), the range of q is

$$2xK_p^{*2}(1 + x) < q < \frac{K_p^{*2}(1 + x)^2}{2\left(1 + K_i^*\right)}. \tag{35}$$

Namely,

$$\frac{\frac{K_p^{*2}(1+x)^2}{2\left(1+K_i^*\right)}}{2xK_p^{*2}(1 + x)} = \frac{1 + x}{4x\left(1 + K_i^*\right)} > 1. \tag{36}$$

Combined with the relationship described in (34), the range for x can be derived as

$$0 < x \leq \frac{1}{4}. \tag{37}$$

With (29) and (30), the maximum q can be found

$$q < \frac{\left(1 + K_i^*\right)(1 + x)}{4}. \tag{38}$$

Therefore, the biggest x, one-fourth, can be selected to have the largest q. Namely, T_d^* can be determined by K_p^* as

$$T_d^* = \frac{1}{4}K_p^*. \tag{39}$$

With (34), the maximum q that satisfies $\gamma_i > 2$ $(i = 1,\ 2,\ 3,\ 4)$ can be found as

$$q < \frac{\left(1 + K_i^*\right)(1 + x)}{4} < \frac{25}{64} \approx 0.391. \tag{40}$$

As same as the IP controller design, K_i^* is decreased from its maximum value one-fourth to zero during the search of the time responses with zero overshoot and maximum possible K_i^*. Similarly, with the specific q and K_i^* and the relationship of

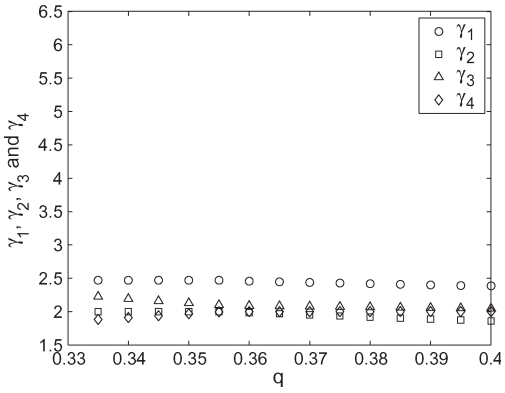

Fig. 6. Desired γ_1, γ_2, γ_3, and γ_4 for the m-IP control.

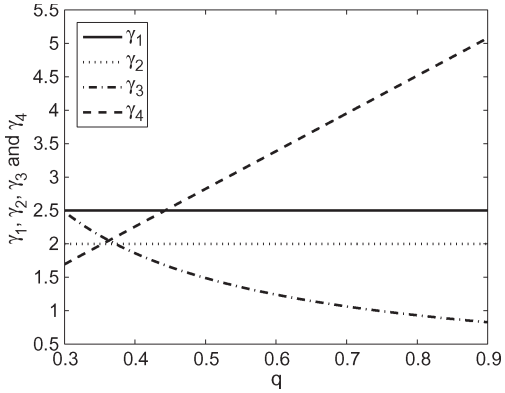

Fig. 7. γ_1, γ_2, γ_3, and γ_4 with the designed m-IP controller.

$T_d^* = K_p^*/4$, the values of K_p^* are calculated by letting $\gamma_1 = 2$, $\gamma_2 = 2$, $\gamma_3 = 2$, and $\gamma_4 = 2$. As shown in Fig. 6, the values of the desired γ_1 and γ_2 are also around 2.5 and 2, respectively. Therefore, the initial parameter setting for the m-IP controller can be determined by letting $T_d^* = K_p^*/4$ and $\gamma_1 = 2.5$, $\gamma_2 = 2$ in (24) and (25), respectively. Namely

$$K_i^* = \frac{4}{21}, \quad K_p^* = \frac{5}{21}\sqrt{10}, \quad T_d^* = \frac{K_p^*}{4}. \tag{41}$$

The characteristic ratios by using the aforementioned initial setting are shown in Fig. 7 with various inertia ratios q. It can be seen that γ_3 decreases dramatically and becomes smaller than 2 when q is larger than 0.372. However, the characteristic ratios with lower indices i, γ_1 and γ_2, are taken as 2.5 and 2, respectively, which have a dominant influence on the overshoot. Unless γ_3 is too small, sufficient damping can still be provided by the designed m-IP controller. In addition, since

$$K_p^* - T_d^* K_i^* = \frac{5}{21}\sqrt{10}\left(1 - \frac{1}{4}\cdot\frac{4}{21}\right) > 0 \tag{42}$$

the designed m-IP control system is stable as explained in the previous section of stability analysis.

The step responses of the normalized m-IP control systems are shown in Fig. 8 under the initial setting of K_i^*, K_p^*, and T_d^*, which are determined by the aforementioned criterion. Compared with the IP control, the damping is obviously improved. Even for q larger than 25/64, such as $q = 0.5$, the time response is satisfactory with small overshoot and short settling time.

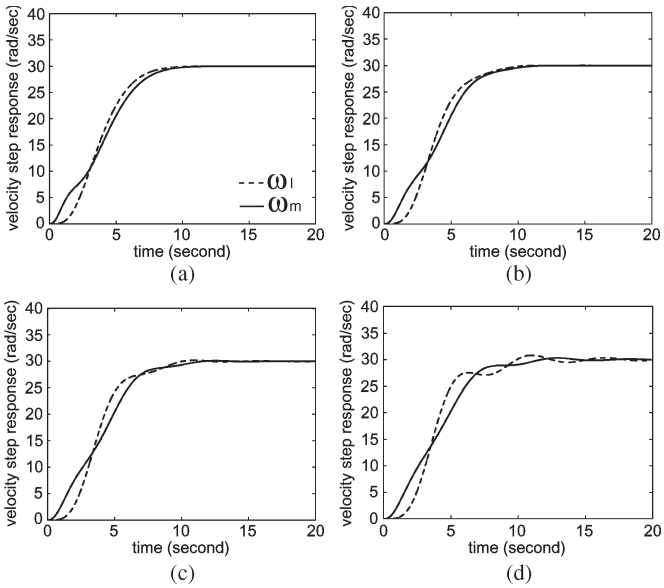

Fig. 8. Velocity step responses with various q's by the m-IP control. (a) $q = 1/3$. (b) $q = 0.5$. (c) $q = 0.6$. (d) $q = 0.7$.

When q further increases, as shown in the cases of $q = 0.6$ and $q = 0.7$, the value of γ_3 is too small for keeping sufficient damping, which causes the corresponding time responses to become oscillatory.

C. m-IPD Controller

In order to improve damping for a large inertia ratio q, the D controller can be added as shown in Fig. 2(c). For the m-IPD control loop, the characteristic ratios are

$$\gamma 1 = \frac{K_p^{*2}}{K_i^*\left(1 + K_i^* + K_d^*\right)} \tag{43}$$

$$\gamma_2 = \frac{\left(1 + K_i^* + K_d^*\right)^2}{K_p^*\left(T_d^* + K_p^*\right)} \tag{44}$$

$$\gamma_3 = \frac{\left(T_d^* + K_p^*\right)^2}{\left(q + K_d^*\right)\left(1 + K_i^* + K_d^*\right)} \tag{45}$$

$$\gamma_4 = \frac{\left(q + K_d^*\right)^2}{T_d^* q\left(T_d^* + K_p^*\right)}. \tag{46}$$

From the analysis of the IP and m-IP controller design, it can be found that assigning the characteristic ratios to be $\gamma_1 = 2.5$, $\gamma_2 = 2$, $\gamma_3 = 2$, and $\gamma_4 = 2$ would give desired time responses with nearly zero overshoot and short settling time. The four parameters of m-IPD controller, K_p^*, K_i^*, K_d^*, and T_d^*, can be directly calculated by solving the nonlinear equations under the aforementioned characteristic-ratio assignment. As shown in Fig. 9, the time responses for a large q, such as 0.7 and 0.9, are significantly improved with the m-IPD controllers, which indicates a more sufficient damping of the designed control system.

However, the values of K_d^* calculated by letting $\gamma_1 = 2.5$, $\gamma_2 = 2$, $\gamma_3 = 2$, and $\gamma_4 = 2$ are negative numbers, which means a positive feedback of the D control signal (see Fig. 10). For a

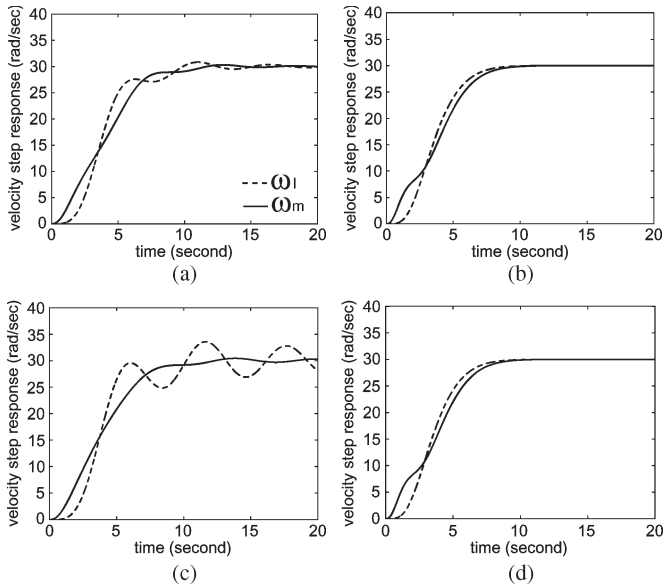

Fig. 9. Comparison of velocity step responses by m-IP and m-IPD control with a large q. (a) $q = 0.7$ (m-IP). (b) $q = 0.7$ (m-IPD). (c) $q = 0.9$ (m-IP). (d) $q = 0.9$ (m-IPD).

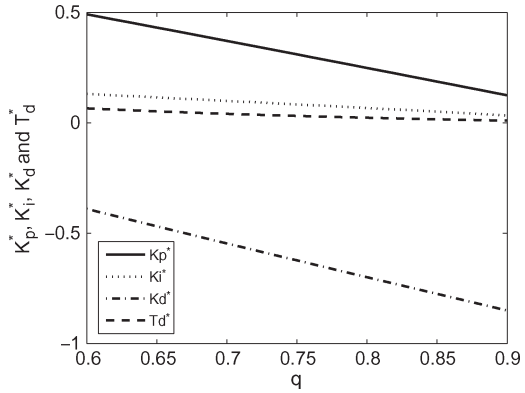

Fig. 10. Parameters of m-IPD controller calculated by characteristic-ratio assignment.

large q, a greater damping, i.e., phase lag rather than phase lead, is needed to suppress the resonance vibrations; therefore, the negative K_d^* becomes necessary. The positive feedback would lead to a very poor robustness of the control system. Although the m-IPD control has satisfactory time responses in simulation, it is impractical for real applications as verified in the following experimental results.

IV. Experimental Results

The configuration of the whole experimental system is shown in Fig. 11. The test bench is controlled by a PC with a 1.6-GHz Pentium IV CPU and a 512-MB memory. Real-time operating system RTLinux is used to guarantee the timing correctness of the real-time tasks. The control programs are written in RTLinux C threads, which can be executed with the strict timing requirement of control sampling time. A 12-b Analog-to-Digital/Digital-to-Analog multifunctional board is used with 10-μs conversion time per channel. All the experiments were carried out under the sampling time of 0.001 s.

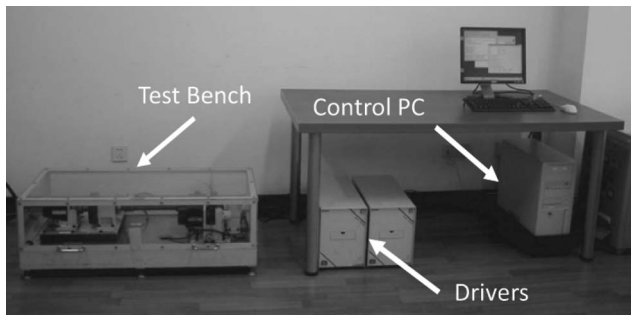

Fig. 11. Configuration of the experimental system.

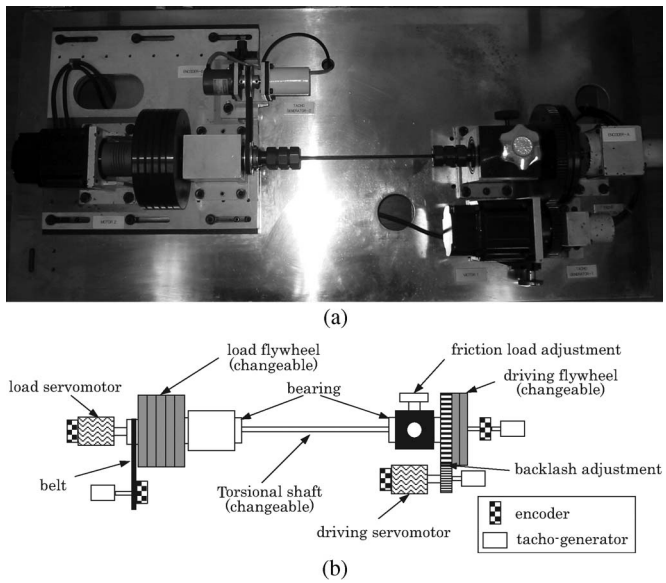

Fig. 12. Experimental setup of the test bench.

TABLE II
Shaft Elastic Coefficients With Various Diameters

Shaft: 4mm	$2.4504(Nm/rad)$
Shaft: 8mm	$3.9207 \times 10^1(Nm/rad)$
Shaft: 12mm	$1.9849 \times 10^2(Nm/rad)$
Shaft: 16mm	$6.2731 \times 10^2(Nm/rad)$
Shaft: 20mm	$1.5315 \times 10^3(Nm/rad)$

The test bench is a torsional system, which can be used to emulate the two-mass system. As shown in Fig. 12, the flywheels of drive side and load side are connected with a long torsional shaft, while the drive torque is transmitted from the drive servomotor to the shaft by gears with a gear ratio of $1:2$ $(N_g = 2)$. The two motor encoders (8000 pulses/rev) are used as rotary velocity sensors with coarse quantization ± 0.7854 rad/s.

For the torsional system, its parameters of gear inertia, load inertia, shaft elastic coefficient, friction load, and gear backlash angle are adjustable. For the sake of simplicity, in the experiments, the friction load and gear backlash angle were being set to their minimum values except in the last experiment for the verification of m-IPD control's robust performance. There are five shafts with different diameters for emulating various the shaft elastic coefficients K_s, as shown in Table II.

TABLE III
INERTIAS OF FLYWHEELS AND MOTORS ON THE DRIVE AND LOAD SIDES

Drive servomotor J_{m0}	$6.5338 \times 10^{-4}(Kg \cdot m^2)$
Drive side basic J_{m1}	$6.1342 \times 10^{-3}(Kg \cdot m^2)$
Drive flywheel J_{m2}	$3.6573 \times 10^{-3}(Kg \cdot m^2)$ (each)
Load side basic J_{l0}	$4.1062 \times 10^{-3}(Kg \cdot m^2)$ (including load servomotor)
Load flywheel J_{l2}	$3.7878 \times 10^{-3}(Kg \cdot m^2)$ (each)

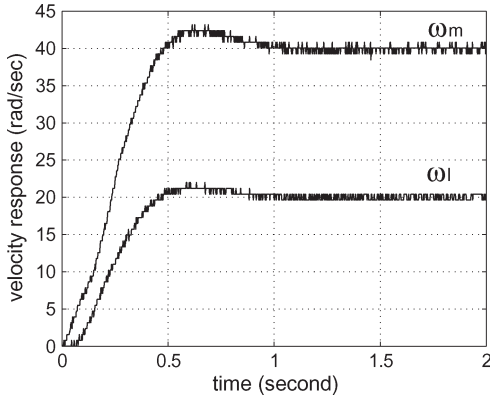

Fig. 13. Velocity step responses with small $q = 0.2751$ (IP control with zero drive flywheel and five load flywheels).

The inertia ratio q can be adjusted by changing the number of attached flywheels on the drive and load sides. The inertia for each component is shown in Table III. The parameters for the emulated two-mass system can be calculated as

$$J_m = J_{m0} + \frac{J_{m1} + mJ_{m2}}{N_g^2} \tag{47}$$

$$J_l = \frac{J_{l0} + nJ_{l2}}{N_g^2} \tag{48}$$

where m and n are the numbers of the flywheels on the drive and load sides, respectively. There are two drive flywheels and five load flywheels in total. Therefore, the range of inertia ratio q that can be emulated is from 0.2751 to 0.7964.

The maximum torque that the drive servomotor can deliver is ± 3.84 N $\cdot$ m. In order to avoid a large saturation of the output torque, the thinnest shaft (4 mm) is chosen, by which the two-mass system has the lowest antiresonance frequency ω_a. Therefore, the real controller parameters K_p, K_i, K_d, and T_d are also small when converting from their normalized values [refer to (7)–(10)]. It should be noticed that the real dynamics of the torsion test bench is obviously much more complex than the dynamics of the ideal two-mass system, particularly with the existence of friction and gears. The experimental velocity responses with various q's are shown in Figs. 13 and 14. Due to the unmodeled dynamics, the experimental results slightly deviate from the time responses in the simulation. However, the experimental results still clearly show that for a small q, 0.2751, the IP controller is enough; for a larger q, 0.6705, the m-IP controller is more effective; while for a large q, 0.7964, both the IP and m-IP controllers are not effective anymore. However, the responses of the m-IP control are better because the controller can provide greater damping than the IP controller.

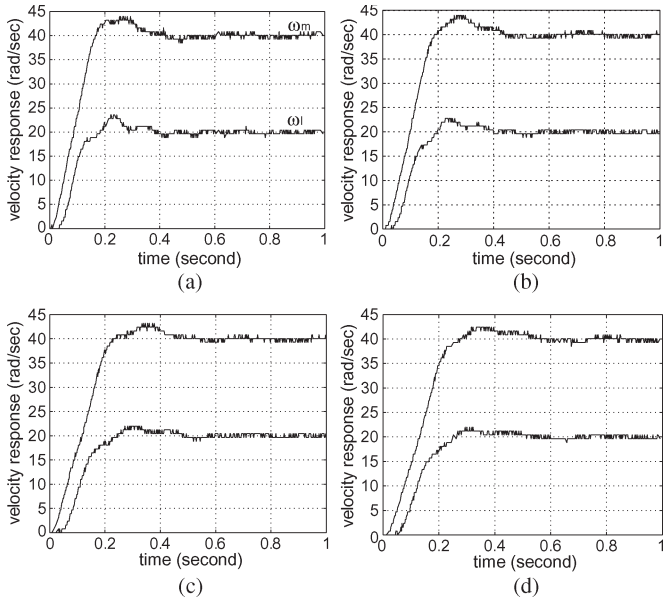

Fig. 14. Velocity step responses with large q. (a) $q = 0.7964$ (IP control with two drive flywheels and zero load flywheel). (b) $q = 0.7964$ (m-IP). (c) $q = 0.6705$ (IP control with two drive flywheels and one load flywheel). (d) $q = 0.6705$ (m-IP).

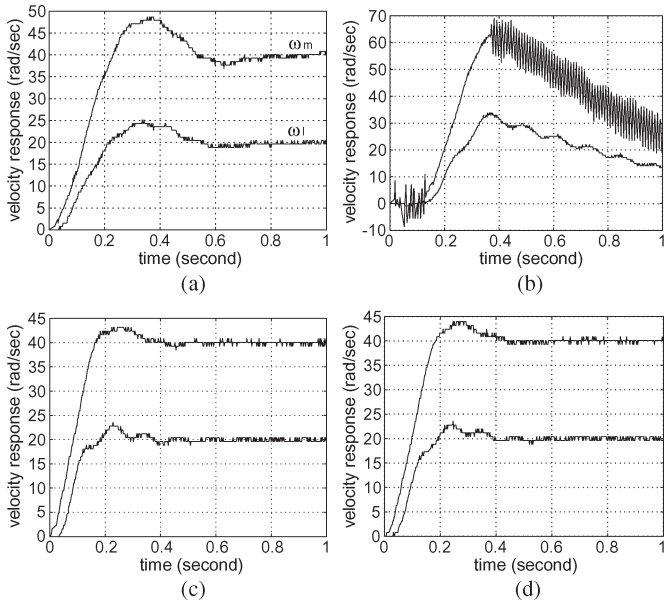

Fig. 15. Robustness of controllers against gear backlash ($q = 0.7964$). (a) m-IPD without backlash. (b) m-IPD with backlash. (c) IP with backlash. (d) m-IP with backlash.

The experimental results in Fig. 15 clearly verify the poor robustness of the m-IPD controller with the negative K_d. With the existence of a large gear backlash, the m-IPD control system actually becomes unstable, while the IP and m-IP control show a much better robustness against the gear backlash nonlinearity, even their time responses are not satisfactory when the inertia ratio q is large, such as $q = 0.7964$.

V. CONCLUSION

In this paper, various low-order PID controllers, the IP, m-IP, and m-IPD controllers, have been designed for the speed

control of the two-mass system based on the normalized model and polynomial method. In order to have sufficient damping, the parameters of the controllers are determined through characteristic-ratio assignment under the principle that all the characteristic ratios should be larger than two. Additional limitations arise from the presence of the two resonance modes, which requires larger characteristic ratios, particularly the ratios with lower indices. In addition, with an increasing inertia ratio, it becomes more difficult to provide sufficient damping through the design of control system.

Based on the aforementioned principle of characteristic-ratio assignment, it is found that for an inertia ratio smaller than one-third, the IP controller can effectively suppress the vibrations with proper damping, while for a relatively larger inertia ratio, the m-IP controller with an additional low-pass filter is effective. For the IP controller design, the initial parameters can be determined by letting $\gamma_1 = 2.5$ and $\gamma_2 = 2$, while for the m-IP controller, the design criterion of $\gamma_1 = 2.5$, $\gamma_2 = 2$, and $T_d^* = K_p^*/4$ is proposed. The m-IPD control is theoretically effective for a large inertia ratio. However, the necessity of a negative derivative gain leads to a very poor robustness. Both simulation and experimental results verified the effectiveness of the designed IP and m-IP controllers when the inertia ratio is relatively small. For the m-IPD controller, its poor robustness is demonstrated by introducing a large gear backlash in experiments. At the same time, the IP and m-IP controllers show promising results of a much better robustness against the gear backlash nonlinearity.

Future works may include a more systematic discussion on the robustness of the IP and m-IP controllers designed by the aforementioned polynomial method, as well as the justification of the controller design by using classical analysis techniques such as root locus, Bode plot, etc. Comparison with the controllers designed by the existing approaches could further enhance the usefulness of the polynomial method. Since the IP controller can be considered as a special m-IP controller with zero-order low-pass filter, the controller design for the two-mass system could be generalized as designing a m-IP controller with the proper selection of low-pass filters. As explained earlier, for a large inertia ratio, the m-IP controller with the first-order low-pass filter becomes less effective. In this case, a fractional-order m-IP controller, which has a low-pass filter with the order between one and two, might provide a better tradeoff between stability and damping. The generalization of controller design for the two-mass system speed control based on fractional-order control could be an interesting research topic.

The corelationship between the characteristic ratios and the damping of the control loop makes the polynomial method promising as a general design method for controlling other more complicated and realistic systems, such as the two-mass system with the availability of the load velocity feedback in which the actuator and sensor are noncollocated. In the new application area of motion control, electric vehicles, with the control bandwidth, increase due to the substitution of engines with electric motors, the vibration control of the electrified drive systems might be a good target for applying the method.

REFERENCES

[1] E. Omine, T. Goya, U. Akie, T. Senjyu, A. Yona, N. Urasaki, and T. Funabashi, "Torsional torque suppression of decentralized generators using $H\infty$ observer," *Renewable Energy*, vol. 35, no. 9, pp. 1908–1913, Sep. 2010.

[2] R. Dhaouadi, K. Kubo, and M. Tobise, "Two-degree-of-freedom robust speed controller for high-performance rolling mill drives," *IEEE Trans. Ind. Appl.*, vol. 29, no. 5, pp. 919–926, Sep./Oct. 1993.

[3] K. Sugiura and Y. Hori, "Vibration suppression on 2- and 3-mass system based on the feedback of imperfect derivative of the estimated torsional torque," *IEEE Trans. Ind. Electron.*, vol. 43, no. 1, pp. 56–64, Feb. 1996.

[4] M. Hirata, K. Z. Liu, and T. Mita, "Active vibration control of a 2-mass system using μ-synthesis with a descriptor form representation," *Control Eng. Pract.*, vol. 4, no. 4, pp. 545–552, Apr. 1996.

[5] S. N. Vukosavić and M. R. Stojić, "Suppression of torsional oscillations in a high-performance speed servo drive," *IEEE Trans. Ind. Electron.*, vol. 45, no. 1, pp. 108–117, Feb. 1998.

[6] R. Muszynski and J. Deskur, "Damping of torsional vibrations in high-dynamic industrial drives," *IEEE Trans. Ind. Electron.*, vol. 57, no. 2, pp. 544–552, Feb. 2010.

[7] L. Wang and Y. Frayman, "A dynamically generated fuzzy neural network and its application to torsional vibration control of tandem cold rolling mill spindles," *Eng. Appl. Artif. Intell.*, vol. 15, no. 6, pp. 541–550, Dec. 2002.

[8] K. Lee and F. Blaabjerg, "An improvement of speed control performances of a two-mass system using a universal approximator," *Elect. Eng.*, vol. 89, no. 5, pp. 389–396, May 2007.

[9] T. Orlowska-Kowalska and K. Szabat, "Control of the drive system with stiff and elastic couplings using adaptive neuro-fuzzy approach," *IEEE Trans. Ind. Electron.*, vol. 54, no. 1, pp. 228–240, Feb. 2007.

[10] T. Orlowska-Kowalska and K. Szabat, "Neural-network application for mechanical variables estimation of a two-mass drive system," *IEEE Trans. Ind. Electron.*, vol. 54, no. 3, pp. 1352–1364, Jun. 2007.

[11] T. Orlowska-Kowalska, M. Dybkowski, and K. Szabat, "Adaptive sliding-mode neuro-fuzzy control of the two-mass induction motor drive without mechanical sensors," *IEEE Trans. Ind. Electron.*, vol. 57, no. 2, pp. 553–564, Feb. 2010.

[12] Y. C. Kim, L. H. Keel, and S. P. Bhattacharyya, "Transient response control via characteristic ratio assignment," *IEEE Trans. Autom. Control*, vol. 48, no. 12, pp. 2238–2244, Dec. 2003.

[13] Y. C. Kim, L. H. Keel, and S. Manabe, "Controller design for time domain specifications," in *Proc. 15th IFAC Triennial World Congr.*, Barcelona, Spain, 2002.

[14] P. Naslin, *Essentials of Optimal Control*. Cambridge, MA: Boston Tech. Publ., 1969.

[15] S. Manabe, "Importance of coefficient diagram in polynomial method," in *Proc. 42nd IEEE Conf. Decision Control*, Maui, HI, 2003, pp. 3489–3494.

Chengbin Ma (M'05) received the B.S.E.E. degree from East China University of Science and Technology, Shanghai, China, in 1997, and the M.S. and Ph.D. degrees in electrical engineering from The University of Tokyo, Tokyo, Japan, in 2001 and 2004, respectively.

From 2004 to 2006, he was an R&D Researcher with the Servo Motor Laboratory, FANUC Ltd., Oshino-mura, Yamanashi Prefecture, Japan. Between 2006 and 2008, he was a Postdoctoral Researcher with the Department of Mechanical and Aeronautical Engineering, University of California, Davis. He is a Tenure-Track Assistant Professor of electrical and computer engineering with the University of Michigan–Shanghai Jiao Tong University Joint Institute, Shanghai Jiao Tong University, Shanghai, and has a joint faculty appointment with the Institute of Automotive Engineering, School of Mechanical Engineering, Shanghai Jiao Tong University. His research interests include mechatronics and motion control, electric drives, and control and optimization of renewable and alternative energy systems such as electric vehicles.

Dr. Ma is a member of the American Society of Mechanical Engineers.

Junyi Cao received the B.S. and M.S. degrees from Xi'an Polytechnic University, Xi'an, China, in 2000 and 2003, respectively, and the Ph.D. degree in mechanical engineering from Xi'an Jiaotong University, Xi'an, in 2006.

He is an Assistant Professor with the School of Mechanical Engineering, Xi'an Jiaotong University. His main research interests include dynamic analysis and the fault diagnosis of mechatronic systems, fractional calculus and its applications, and environmental energy harvesting.

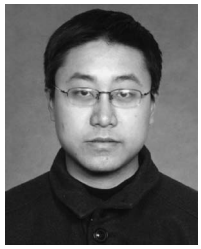

Yue Qiao received the B.S.E.E. degree from the University of Michigan–Shanghai Jiao Tong University Joint Institute, Shanghai Jiao Tong University, Shanghai, China, in 2010, where he is currently working toward the M.S. degree.

His research interests include theory and applications of motion control and mechatronics.